

# Adaptive fuzzy weighted median filter for microcalcifications detection in digital breast tomosynthesis images

Syafiqah Aqilah Saifudin<sup>1</sup>, Siti Noraini Sulaiman<sup>1,2,3</sup>, Muhammad Khusairi Osman<sup>1</sup>, Iza Sazanita Isa<sup>1</sup>,  
Noor Khairiah A Karim<sup>4,5</sup>, Nur Athiqah Harron<sup>1</sup>

<sup>1</sup>Electrical Engineering Studies, College of Engineering, Universiti Teknologi MARA, Cawangan Pulau Pinang, Permatang Pauh Campus, Permatang Pauh, Malaysia

<sup>2</sup>Advanced Rehabilitation Engineering in Diagnostic and Monitoring Research Group (AREDiM), Electrical Engineering Studies, College of Engineering, Universiti Teknologi MARA, Cawangan Pulau Pinang, Permatang Pauh Campus, Permatang Pauh, Malaysia

<sup>3</sup>Integrative Pharmacogenomics Institute (iPROMISE), Universiti Teknologi MARA, Puncak Alam Campus, Puncak Alam, Malaysia

<sup>4</sup>Department of Biomedical Imaging, Advanced Medical and Dental Institute, Universiti Sains Malaysia, Kepala Batas, Malaysia

<sup>5</sup>Breast Cancer Translational Research Programme (BCTRTP), Advanced Medical and Dental Institute, Universiti Sains Malaysia, Kepala Batas, Malaysia

## Article Info

### Article history:

Received Nov 21, 2023

Revised Jan 30, 2024

Accepted Feb 16, 2025

### Keywords:

Breast cancer

DBT enhancement

Digital breast tomosynthesis

Fuzzy weighted median filter

Microcalcification detection

## ABSTRACT

Breast cancer is a global leading cause of female mortality. Digital breast tomosynthesis (DBT) is pivotal for early breast cancer detection, with microcalcifications serving as crucial indicators. However, the movement of the DBT machine introduces blurry artefacts, potentially impacting accurate diagnosis. This study addresses this challenge by proposing an adaptive fuzzy weighted median filter (AFWMF) to enhance DBT images and aid microcalcification diagnosis. AFWMF automatically determines optimal parameters based on input images, outperforming conventional methods with a threshold range (C) from peak to end of switching. Quantitative assessment reveals peak signal to noise ratio (PSNR), and mean absolute error (MAE) values of 96.2267 and 0.0000636, respectively, demonstrating a significant improvement in microcalcification detection. This study contributes an effective and adaptive enhancement technique for DBT images, promising better breast cancer diagnosis, particularly in microcalcification scenarios.

This is an open access article under the [CC BY-SA](https://creativecommons.org/licenses/by-sa/4.0/) license.



## Corresponding Author:

Siti Noraini Sulaiman

Electrical Engineering Studies, College of Engineering, Universiti Teknologi MARA

Cawangan Pulau Pinang, Permatang Pauh Campus

13500 Permatang Pauh, Penang, Malaysia

Email: sitinoraini@uitm.edu.my

## 1. INTRODUCTION

Breast cancer is the most common disease that affects women worldwide and is the leading cause of death for women aged 35 and above. Notably, 66% of women diagnosed with breast cancer are over the age of 55 [1]. Calcifications, which are small clusters of calcium deposits that develop in breast tissues and appear as white spots inside the breast area on mammograms and digital breast tomosynthesis (DBT) images, are the early indicators of these tumours [2]. Calcifications are classified into two types: macrocalcifications and microcalcifications. Macrocalcifications larger than 1 mm are generally non-cancerous and can be treated directly. However, microcalcifications, being another type, require additional screening due to the fact that they may signify cancer, necessitating closer observation [1]. Early detection of microcalcifications is crucial, as they are an early sign of breast cancer, and significantly improve a patient's chances of survival. Studies indicate that 99% of cases survive within 5 years with early detection [1], [3].

Detecting calcifications can be challenging due to their small size as these calcium compounds are microscopic. During the breast screening process, mammograms and DBT images are frequently employed. DBT is a cutting-edge technology that produces three-dimension (3D) screening images of the breast area, providing multiple angles view [4]. 10 to 30 projection images within a limited angle range of approximately  $11^\circ$  to  $60^\circ$  are required [5]. Furthermore, compared to mammogram images, DBT images offer the advantage of reducing false positive rates by 6 to 67% due to improved visualization of overlapping breast tissue, which can lead to normal tissue appearing abnormal or suspicious on mammogram images [5]-[7]. As a result, previous researchers have explored various methods for developing models that can detect calcifications in DBT images.

However, the excellent DBT screening technology used to create 3D images has certain drawbacks, including the presence of blurry artefacts. Blurry artefacts are noise that occurs in DBT images during screening. Despite technological advances, this new technology cannot entirely eliminate the presence of blurry artefacts, which are caused by poor positioning, patient movement during screening, and excessive radiation exposure [8]. These factors can reduce the visibility of calcifications in DBT images, necessitating an enhancement stage to remove noise and deblur blurry objects in DBT images in order to see calcifications in the breast region more clearly [8].

Previous research has introduced several algorithms or methods for noise removal from DBT images. For enhancement of the DBT images, various noise filtering and thresholding techniques have been proposed [9]-[17]. Many researchers, however, use unsharp masking to aid their proposed models, such as a deep learning model and use it as the primary proposed enhancement algorithm. Additionally, other researchers have combined the unsharp masking algorithm with a weighted guided filter to enhance the vessel details in mallendoscopic images. Furthermore, another researcher proposed using unsharp masking to improve their proposed deep learning models, ChampNet [18], [19]. In 2022, a study proposed the use of an unsharp masking filter from the research by Panetta *et. al* [20] and Saifudin *et. al* [21] to form several algorithms of non-linear unsharp masking (NLUM) filters [22]. This study introduced and compared two different algorithms of non-linear unsharp to find the best combination of non-linear filters to be used in the NLUM algorithm and produced the best enhancement technique for DBT images [22]. Continuous from this study [22], in 2023 the researcher introduced a fuzzy weighted median filter (FWMF) in the NLUM algorithm which produced better results compared to the previous study in 2022 [22] which showed that FWMF can also enhance DBT images when used in NLUM algorithm [23]. However, from the FWMF algorithm in this study, the FMWF can be improved more to adapt to the DBT images in enhancing the images that might help in the detection of microcalcifications.

From the proposed method introduced [23], the FWMF appears to have some gaps for improvement. Based on the previous study, the researcher proposed the FWMF to improve images contaminated by salt and pepper noise, and this method was also combined with the denoising based (DB) clustering method to produce more efficient enhancement techniques [24]. In prospective studies, these filters demonstrated promising results in enhancing and filtering the targeted image outperforming other filters in comparison. Unlike conventional median filter, this filter used stricter conditions to determine the pixel value to replace the existing pixel value in the enhancement process, rather than simply finding the median of all pixels in a 3-by-3 window as the conventional median filter does [24].

The FWMF is a modified median filter technique that leverages the fuzzy membership function to weight the median filter algorithm in replacing the pixel value in order to improve the image [24], [25]. Toh *et al.* [25] modified the median filter by including a fuzzy membership function in the median algorithm. The difference in this algorithm is that the normalization step in the fuzzy membership function now uses the range that was specifically selected from the image histogram [25]. In their study, the normalization range was fixed to 10 to 30 it exhibited switching behaviour within the range [25].

However, it should be noted that since each image's histogram may process different and unique switching ranges, using fixed normalization ranges in the fuzzy algorithm may require adjustments. Moreover, as indicated in the study by Toh *et al.* [25], the selection of range from 10 to 30 remains unclear in determining the most suitable range for the algorithm. The extent to which the normalization range can extend until reaching a certain pixel value or length also lack a clarity. Furthermore, the limitation of this method is evident as it primarily focusses on non-medical images, with no research conducted on medical images, particularly DBT images, despite the introduction of DBT as a new breast area screening technique [25]. The lack of research on DBT images highlights the need for exploring and evaluating this filtering technique in a medical imaging context, specifically for breast cancer detection.

Therefore, due to existing limitations and to the best of our knowledge, the absence of research on DBT images using this filtering technique, the proposed adaptive fuzzy weighted median filter (AFWMF) is introduced in this paper. AFWMF is designed to overcome the limitations of the conventional FWMF and is compared with it as a part of this study.

**2. METHOD**

The FWMF is a filter previously proposed for improving portrait images using the median filter. It achieves this by incorporating the fuzzy membership function to weight the median filter. However, as this technique was originally intended for portrait images and its optimal range for image enhancement remained uncertain in a previous study, adaptations are necessary to suit DBT images or any medical images. As a result, this study takes advantage of this opportunity to investigate the best threshold range to be used in enhancing DBT images while determining the optimal values of  $T_1$  and  $T_2$  based on the histogram switching of the DBT images. To tailor the algorithm of DBT images, this study modifies the existing FWMF in portrait images. The whole process of the enhancement technique is clearly portrayed in Figure 1 and the modification is known as the AFWMF is illustrated in Figure 2. Further explanation is provided in the following subsection.

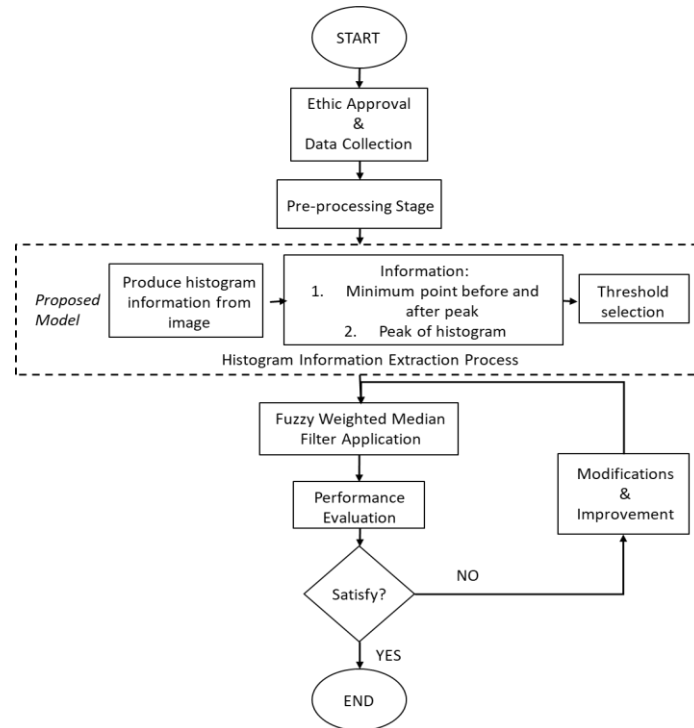


Figure 1. The overall process of the AFWMF for proposed filtering method

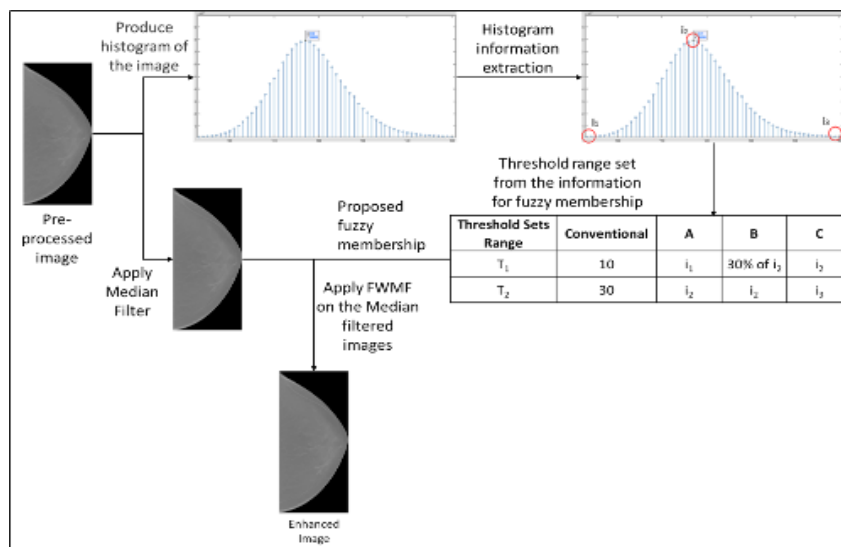


Figure 2. Flow chart of the proposed filtering method of AFWMF in this study

### 2.1. Ethical approval and data collection

The ethical application to Universiti Sains Malaysia's Jawatankuasa Etika Penyelidikan Manusia (JEPeM) is the first step in this project. Before the study began, the ethical application for DBT data collection with code study: USM/JEPeM/21090622 was approved. The images are collected using the picture archiving and communication system (PACS) at the Advanced Medical and Dental Institute (AMDI), Bertam at the USM Imaging Unit with the assistance of a trained radiographer. Furthermore, the images are deidentified and anonymized before being made public in accordance with ethical guidelines. The input images are DBT images collected from two patients, totaling eleven DBT images. The DBT images were imported into the MATLAB R2020a software as DICOM images, which were then converted to bitmap images to run smoothly in the MATLAB software. These images will then go through pre-processing steps, which are critical for preparing DBT images before they enter the enhancement stage.

### 2.2. Pre-processing stage

The preprocessing step had been done to prepare the images before entering the proposed algorithm. This step is crucial in facilitating the enhancement procedure by eliminating background objects in the DBT images that may appear outside the breast area. Additionally, the present of pectoral muscle, which connected the shoulder and breast area, is also be eliminated. Darker and almost black objects, as well as the background are set to totally black intensity or zero-pixel value.

### 2.3. Histogram information extraction

From the preprocessing stage, the DBT images produce a histogram graph of intensity counts over the intensity values. Then the system automatically detects the intensity value that has the highest count, and this value is set as  $i_2$  which represents the peak. Subsequently, from the peak, the negative gradient is detected on both sides until reaching the lowest count from the peak. The intensity value before the peak is set as  $i_1$ , and the intensity value after the peak is set as  $i_3$ . The position of  $i_1$ ,  $i_2$ , and  $i_3$  are depicted in Figure 3.

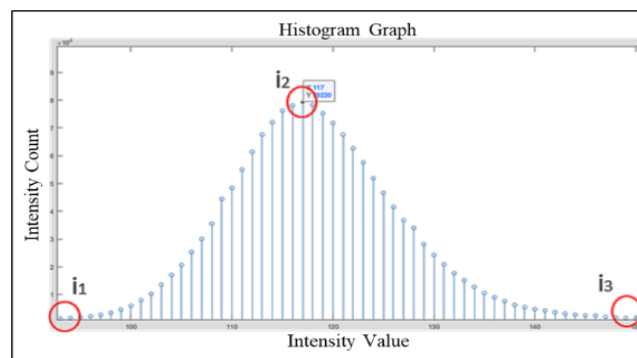
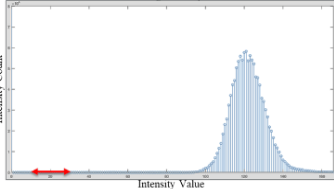
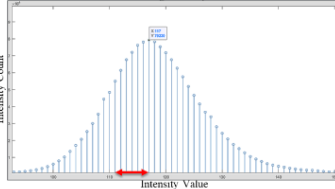
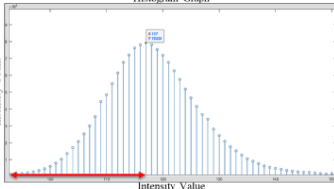
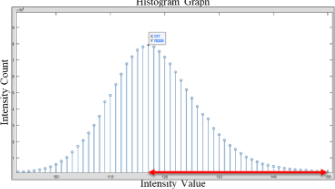


Figure 3. The position of  $i_1$ ,  $i_2$ , and  $i_3$  in histogram graph

In the fuzzy membership function represented by (5), the values of  $T_1$  and  $T_2$  are essential to complete this process. Toh *et al.* [25] explained,  $T_1$  and  $T_2$  threshold values were initially set to 10 and 30, respectively, to align with the histogram switching of the tested images in their study. However, the previous study was unsure of the range that should be used to achieve better image enhancement results, but it chose to use this range. As a result, this study takes advantage of this opportunity to investigate the best range of threshold to be used in enhancing DBT images while determining the best value of  $T_1$  and  $T_2$  based on the DBT images' histogram switching.

This study proposed that these  $T_1$  and  $T_2$  values will regulate the intensity value based on a histogram graph that varies with the image intensity counts. These three intensity values were automatically extracted and will then be combined to form three sets of threshold ranges that will be tested on DBT images using the AFWMF. The threshold ranges as portrayed in Table 1 were labelled as range A, range B, and range C which start with  $i_1$  to  $i_2$ , 30% of  $i_2$  to  $i_2$ , and  $i_2$  to  $i_3$  respectively. The outcome of the filter, which is influenced by the varied threshold sets, will be compared to each other as well as the conventional threshold ranges of 10 and 30 for  $T_1$  and  $T_2$ , respectively. This comparison will provide insights into the performance of the AFWMF with different threshold settings and enable the selection of the most suitable threshold ranges for enhancing DBT images.

Table 1. The labelled switching position on the histogram

Threshold	Histogram	Threshold	Histogram
Conventional		B	
	<p>Threshold range fixed from 10 to 30</p>		<p>Threshold range from 30% <math>i_2</math> to <math>i_2</math></p>
A		C	
	<p>Threshold range from <math>i_1</math> to <math>i_2</math></p>		<p>Threshold range from <math>i_2</math> to <math>i_3</math></p>

**2.4. Fuzzy weighted median filter**

A FWMF is a filtering technique that utilizes a fuzzy algorithm with specific conditions to determine the optimal weight to allocate to the median filter. The algorithms will consider all of the 8-neighboring windows of a targeted pixel, which are marked in red as shown in Figure 4. The FWMF algorithm begins by calculating the difference between the values in each of the 8-window neighbors and the targeted pixel in the center, denoted as  $I(i,j)$ . The value of this operation was then declared as  $d(i,j)$ , which was later found to be its maximum absolute value,  $D(i,j)$ . This maximum absolute value,  $D(i,j)$ , was used by the fuzzy membership function to determine the fuzzy value ranging from 0 to 1. The algorithm for the FWMF began with the linearly fuzzy weighted correction value equation, and then the median filter algorithm, input images, and fuzzy membership function were used to fill this (1). The linearly fuzzy weighted correction value can be determined as [24].

$$F(i, j) = [1 - F_1(i, j)] \cdot I(i, j) + F_1(i, j) \cdot M(i, j) \tag{1}$$

Firstly, the algorithm starts with the finding of the median filter executed from the input images. The median filter can be determined in (2).

$$M(i, j) = median\{I(i + k, j + l)\} \text{ as } k, l \in (-1,0,1) \tag{2}$$

The input image was then used to calculate the absolute luminance difference by subtracting each of the 8-neighbour windows from the targeted pixel. The results of the subtraction process are then expressed in absolute values. The absolute luminance difference is measured in (3).

$$d(i + k, j + l) = |I(i + k, j + l) - I(i, j)| \text{ with } (i + k, j + l) \neq (i, j) \tag{3}$$

Applying the absolute luminance difference mentioned previously into (4), its maximum value was used to find local information as expressed in (4).

$$D(i, j) = max\{d(i + k, j + l)\} \tag{4}$$

The local information,  $D(i,j)$  obtained earlier was used in applying the fuzzy concept through fuzzy membership function that determines its output value,  $F(i,j)$  based on the maximum absolute luminance difference [24]. The fuzzy membership function can be defines as  $F_1(i,j)$  (5).

$$F_1(i, j) = \begin{cases} 0 & ; D(i, j) < T_1 \\ \frac{D(i, j) - T_1}{T_2 - T_1} & ; T_1 \leq D(i, j) < T_2 \\ 1 & ; D(i, j) \geq T_2 \end{cases} \tag{5}$$

Where  $T_1$  and  $T_2$  threshold values were set as Table 2.

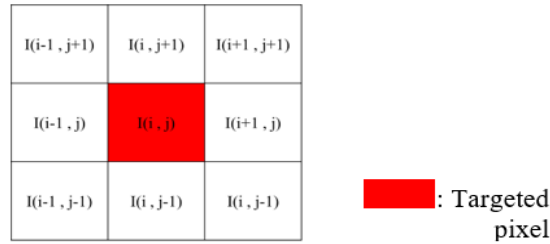


Figure 4. The 8-neighbours window with targeted pixel at centre

Table 2. The information on the threshold value is based on the intensity count in the histogram of the images

Threshold sets range	Conventional	A	B	C
$T_1$	10	$i_1$	30% of $i_2$	$i_2$
$T_2$	30	$i_2$	$i_2$	$i_3$

### 2.5. Performance evaluation

The performance of the proposed filtering method was compared and evaluated using three metrics: mean square error (MSE), peak signal to noise ratio (PSNR), and mean absolute error (MAE), all of which are calculated using the input and output images. The MSE value was used to evaluate PSNR, which is calculated by dividing the square of 255 by the MSE value. After that, the result was inserted into log with base 10 and times with 10. The full PSNR equation portrayed in (6).

$$PSNR = 10 \log_{10} \left( \frac{256^2}{MSE} \right) \quad (6)$$

Following the calculation of PSNR, the MAE was calculated using (7).

$$MAE = \frac{\sum_{i=0}^{M-1} \sum_{j=0}^{N-1} |E(i,j)_{filtered} - I(i,j)_{original}|}{M \cdot N} \quad (7)$$

PSNR and MAE are used to compare the differences and similarities between the output image and the input image. The system that has been analyzed will then be measured, and the best method will be discovered based on these measurements. These measurements' outcomes were compared. The AFWMF is an enhancement technique that used the DBT images' histograms to detect intensity switching for use in the fuzzy membership function. The detected switching as labelled in Table 1, is then sorted into three different threshold range and were used in (5).

## 3. RESULTS AND DISCUSSION

In response to reservations raised in a previous study regarding parameter arrangement in the filter, this study has made adaptations and introduced automatic selection for the required parameter, addressing the previous study's concerns. The aim is to counter the uncertainties regarding parameter selection by automating the process. Toh *et al.* [25], explained the threshold range of  $T_1$  and  $T_2$  in (5) must lie or cover the range of the switching resulting this method can precisely select the range of the threshold value based on their histogram results. DBT images of the breast area typically exhibit bell-shaped graphs and the threshold ranges for the fuzzy switching were labelled as shown in Table 1. The fuzzy algorithm was modified to accommodate DBT images with bell-shaped graphs, which distinguished them from other types of images. This modification enables the fuzzy algorithm to make decisions based on the intensity switching in the histogram graph as shown in Figure 5, and the normalization process is performed only on the intensity values involved in the switching.

Toh *et al.* [25], explained the study's ranges were based on intensity switching of the histogram graph of regular images, rather than medical images such as DBT images. However, the threshold ranges are clearly visible in the switching of the histogram graph, prompting this study to test different types of ranges on a single switching. These ranges include switching from initial to peak, or 30% of peak to peak or initial to final switching. The results obtained from these three ranges differ, particularly in terms of PSNR and MAE values. All of these values were compared and measured to determine the best ranges to use in the fuzzy algorithm. This comparison process aids in selecting the most effective threshold ranges for the enhancement of DBT images. Furthermore, this study tested different types of ranges on a single switching.

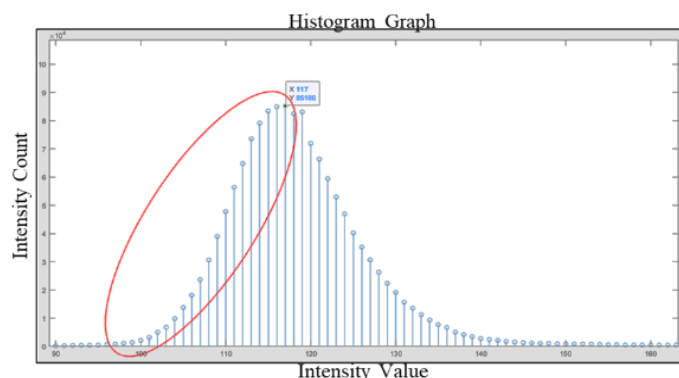


Figure 5. The intensity switching position in the histogram graph

### 3.1. Qualitative analysis

This section presents the results of the proposed filtering method called AFWMF, which align with the study's objective and uses pre-processed images as input to the proposed method. The results of this enhancement technique are shown in Table 3. Due to the general nature of DBT images, histogram switching occurred in intensity values ranging from 80 to 200. The intensity count's lowest value before peak, the peak itself, and the lowest value after the peak are clearly distinct within these ranges. There are 11 images had been tested using these algorithms and each images had their own value of  $i_1$ ,  $i_2$ , and  $i_3$  as portrayed in Figure 6.

The threshold ranges can be alternate to 3 threshold ranges known as A, B and C which investigate the best switching ranges to be used in this AFWMF. Based on Table 3 the results of the proposed filtering methods all had different fuzzy membership function or threshold values that operated on the input images. The AFWMF is formed by using the results of the input images and their histogram information. Any number below the low threshold value is automatically set to zero, while any number above the high intensity value automatically set to one. The numbers within the threshold ranges are normalised to a number between 0 to 1, and these normalized pixel values of the input image are then used in the next step of the AFWMF, which is the median filter algorithm. This step aids in weighting the median filter in the AFWMF for filtering purposes on DBT images.

As shown in Table 3, the outcomes derived from image 1 indicate that the histogram graph exhibits a discernible transition from 103 to 135, a pattern nearly identical to that observed in image 2, image 3, and image 5, where the intensity values form a bell-like shape ranging from 100 to 140. In contrast, image 4 displays a distinct and wider pattern of histogram switching, spanning from 86 to 145, with some fluctuations in intensity values at the onset of the transition. Specifically, in the case of image 4, the value of  $i_1$  reached its lowest point before the rise in switching, evident in the histogram graph at 84.

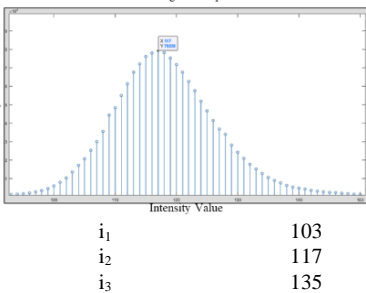
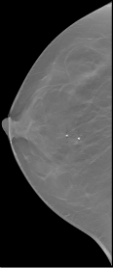
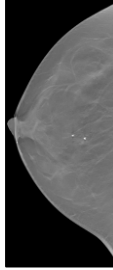
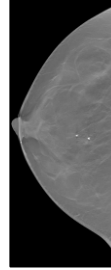
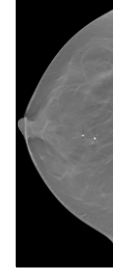
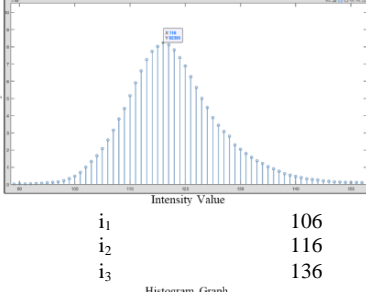
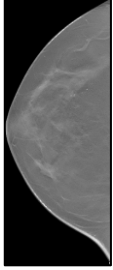
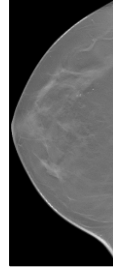
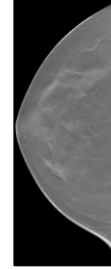
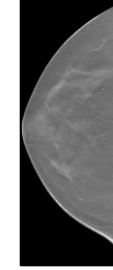
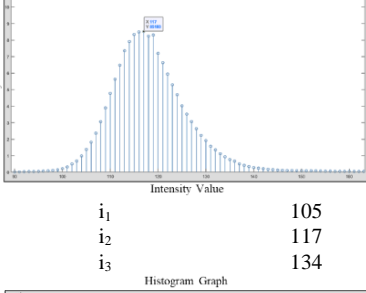
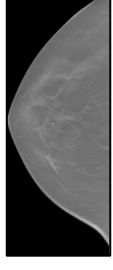
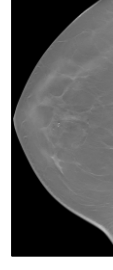
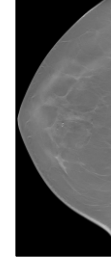
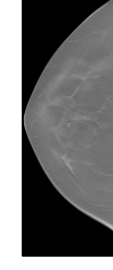
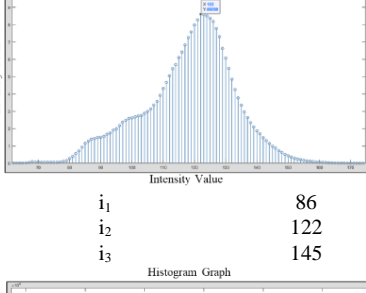
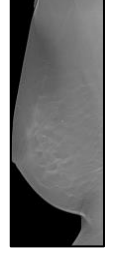
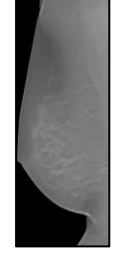
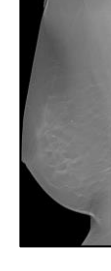
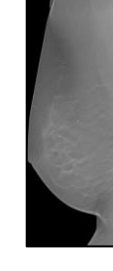
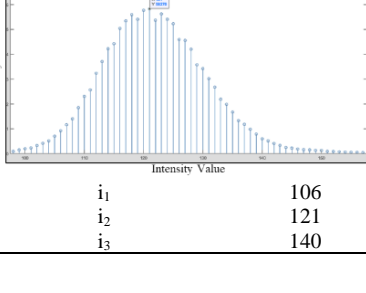
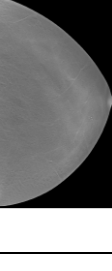
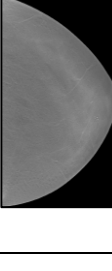
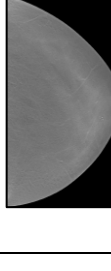
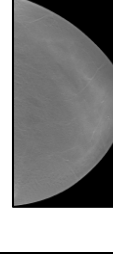
Considering image 1 as the input for the filters, the results reveal that the filter enhances DBT images. However, the proposed method outperforms conventional methods, evident in the enhanced clarity of calcifications in the output image compared to the input images. Among the output images, AFWMF with range C (AFWMF C) stands out for producing clearer calcifications with a dimmer background than other filters. This enhancement facilitates calcification detection, as the calcifications are distinctly visible while the background is dimmed, enhancing the overall image quality. For a more comprehensive comparison, it is noteworthy that image 2, image 3, and image 5 contain smaller calcifications than image 1 and image 4. Consequently, distinguishing results through visual observation is challenging, underscoring the efficacy of the proposed method in enhancing images over conventional methods.

In images 2, 3, and 5, the calcifications, though small, are effectively enhanced by the filter, even when blending with background objects like breast mass and breast gland. The filter enhances DBT images while increasing calcification visibility, with AFWMF C yielding the dimmest background and the clearest calcifications. In contrast, image 4 presents a unique perspective, characterized by a brighter area, making it challenging to differentiate between calcifications and other objects. The proposed method successfully enhances input images, with AFWMF C offering the most optimal results as it produces a slightly dimmer background and brighter calcifications compared to other filters.

Despite variations in the characteristics of input images, the proposed method introduces a filter capable of automatically optimizing parameters in the algorithm, accommodating diverse parameter values for different images. This flexibility demonstrates the ability of the proposed algorithm to enhance images featuring various breast characteristics effectively. The results underscore that using range C in the fuzzy algorithm enhances the visibility of calcifications in DBT images, producing brighter calcifications compared to other ranges. While the output images may not exhibit significant variation across different normalization

threshold ranges, quantitative assessments using MAE and PSNR prove instrumental in discerning subtle differences. The discussion on determining the optimal threshold range for histogram switching to enhance DBT images will follow in the subsequent section.

Table 3. The results produced from the four (4) algorithms of conventional FWMF and AFWMF with different threshold ranges

Input Image	Histogram of the input images	Conventional	AFWMF A	AFWMF B	AFWMF C
Image 1	 <p><math>i_1</math> 103 <math>i_2</math> 117 <math>i_3</math> 135</p>				
Image 2	 <p><math>i_1</math> 106 <math>i_2</math> 116 <math>i_3</math> 136</p>				
Image 3	 <p><math>i_1</math> 105 <math>i_2</math> 117 <math>i_3</math> 134</p>				
Image 4	 <p><math>i_1</math> 86 <math>i_2</math> 122 <math>i_3</math> 145</p>				
Image 5	 <p><math>i_1</math> 106 <math>i_2</math> 121 <math>i_3</math> 140</p>				



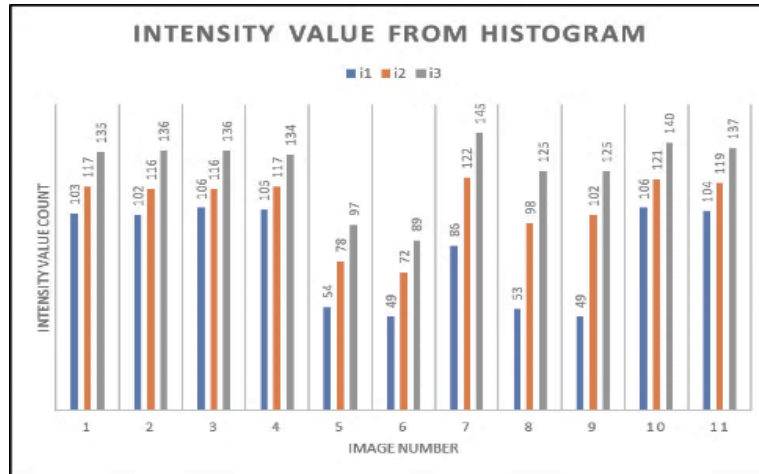


Figure 6. The chart of the  $i_1$ ,  $i_2$ , and  $i_3$  value for each images tested

### 3.2. Quantitative analysis

The qualitative measure is difficult to use in assessing the performance of enhancement methods since everyone views things from different perspectives. As a result, the quantitative results will provide numerical support for the qualitative results. The quantitative outcomes of this technique are depicted in Table 4. The results in Table 4 shows several quantitative results of the images complementing the output images shown in qualitative analysis subsections before. According to the results, all the proposed techniques outperform the conventional FWMF, and this filtering technique produces PSNR values above 90 quantitatively. The MAE results show that there is not a significant difference between the different threshold ranges, with the majority of the results falling below 0.0001. However, for certain images, the difference is noticeable if the MAE results are greater than 0.0001 at all output images with the exception of image 4. Among all of the results shown, image 1 has the highest PSNR value at 98.5598, which also exceeds the other threshold ranges produced by the same image. On the other hand, the PSNR value produced by image 3 was the lowest when compared to other images produced as a complement to their algorithms.

The proposed methods for threshold C produced the lowest MAE value in two images, as the results for both images produced less than 0.0001 and exactly 0.0001 for image 1 and image 5, respectively. Furthermore, the proposed method demonstrated that it could outperform the conventional FWMF because all of the AFWMF for each threshold range produced lower MAE values than the conventional FWMF, particularly on images 2 and 3, where only the conventional FWMF produced higher than 0.0001 at numbers 0.0003 and 0.0002, respectively.

Table 4. The quantitative results were produced from the 4 algorithms of conventional FWMF and AFWMF with different threshold ranges

Image		Conv	A	B	C
1	Processing time (s)	9.4545	9.0836	9.9069	10.7555
	MSE	0	0	0	0
	PSNR	94.5697	96.8913	97.1605	98.5598
	MAE	0.0001	0.0001	0.0001	0
2	Processing time (s)	8.7382	9.1989	9.566	9.587
	MSE	0	0	0	0
	PSNR	92.9794	97.4296	97.5254	97.9697
	MAE	0.0003	0	0	0
3	Processing time (s)	8.5993	8.8736	9.6389	9.8196
	MSE	0	0	0	0
	PSNR	91.0961	92.3108	92.3281	92.5934
	MAE	0.0002	0.0001	0.0001	0.0001
4	Processing time (s)	12.5236	13.6486	11.8958	13.2634
	MSE	0	0	0	0
	PSNR	93.7456	94.4783	94.7554	95.2906
	MAE	0.0001	0.0001	0.0001	0.0001
5	Processing time (s)	6.2566	6.614	6.7759	6.7616
	MSE	0	0	0	0
	PSNR	93.3928	94.2433	94.2845	94.8717
	MAE	0.0002	0.0002	0.0002	0.0001

Notably, range C proves to be the best threshold range for producing the highest PSNR value, outperforming the conventional FWMF and other threshold ranges. Considering the range used, range C contains the most switching of the histogram graph, containing the greatest changes in intensity count, which included drastically increasing and decreasing the intensity count. In comparison to other ranges, A and B only include half of the switching or 30% of the increase in switching. However, when compared to the range that included half switching, the threshold that contained only 30% of the increase switching produced the highest PSNR value. This demonstrated that it is preferable to include the entire switching in the fuzzy normalization section of AFWMF rather than just a portion of the switching.

These results shows that range C can enhance DBT images the best compared to other range performed in AFWMF. As this range produced the highest PSNR and lowest MAE value, it is safe to say that this techniques with range C can enhance DBT images better than conventional method proposed by previous researcher. While only five images were displayed in this section, a total of eleven images were tested to obtain the PSNR and MAE value. All 11 results of PSNR value are displayed in Figure 7. Unfortunately, due to the low values of the MAE produced by these algorithms, the MAE values for this section had been excluded in this discussion as 5 of the total images portrayed before already discussing the MAE value produced.

Generally, the best results produced is when the images produce higher PSNR and lower MAE value. Based on Table 4, the MSE was not used in this part of the study as the MSE value produced by this technique are lower than 0.00001. The highest PSNR value was obtained for image 6, which was enhanced using range B, with a PSNR value of 100.2264 and a MAE value of 0.9999. On the other hand, image 9, which was enhanced using conventional FWMF, produced the lowest PSNR value of 90.1801 and the highest MAE value. When comparing the overall results, the AFWMF algorithms consistently outperformed the conventional FWMF, with higher average PSNR values and lower average MAE values. Table 5 provides the average PSNR and MAE values for each algorithm, confirming the superior performance of the AFWMF method in enhancing DBT images.

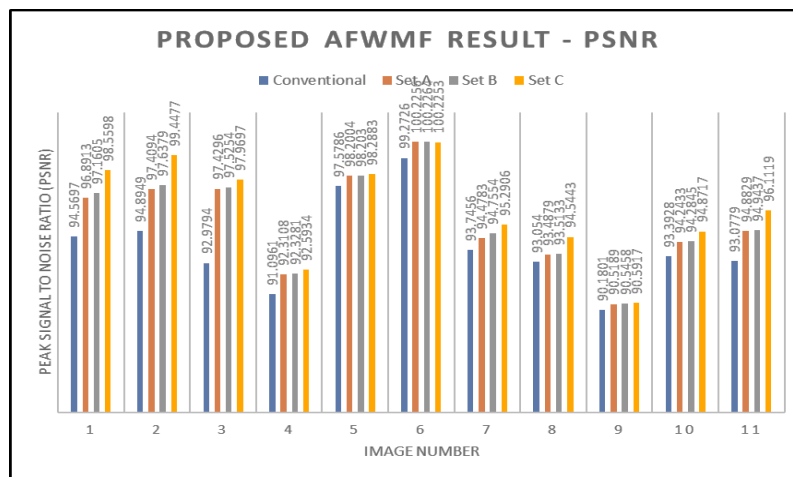


Figure 7. The PSNR results of the eleven (11) images produced using the proposed filtering method

Table 5. The average results of the proposed AFWMF

Image	Conv	A	B	C
Average PSNR	93.985609	95.461673	95.556727	96.226764
Average MAE	0.0001545	9.091E-05	9.091E-05	6.364E-05

Averagely, the result showed that threshold range C produced the best PSNR and MAE averagely which at 96.2268 and 0.9996, respectively. Thus, making this parameter produced the best quantitative results among another parameter for this algorithm. However, the undesirable result was by the conventional threshold ranges at 10 and 30 which making the 93.985609 and 0.0001545 of PSNR and MAE value averagely. This shown that the proposed method can improved from the conventional method. Moreover, the range of threshold A produced the lowest PSNR among the proposed method at 95.461673 and high MAE value at 0.9994636 making this ranges cannot be used in this AFWMF. These findings demonstrate the effectiveness of the proposed AFWMF technique in improving the quality of DBT images and achieving better image enhancement results, which can have significant implications for breast screening and diagnosis.

Within the confines of this investigation, three distinct algorithms were introduced, each characterized by variations in the range implemented within the fuzzy algorithm. Subsequently, these ranges were systematically compared against a conventional method. The method that yielded the highest PSNR value and the lowest MAE value was identified as the most efficacious in enhancing DBT images. Notably, among the proposed methods, it was determined that range C outperformed the conventional method, establishing itself as a superior enhancement technique for DBT images.

The significance of a robust enhancement technique for DBT images cannot be overstated, particularly in the context of calcification detection processes conducted by radiologists or implemented through machine learning algorithms. The empirical findings of this study underscore the effectiveness of the proposed method, specifically utilizing AFWMF C in the fuzzy algorithm. This particular configuration demonstrated exceptional capabilities in enhancing DBT images. This heightened enhancement potential holds considerable promise in augmenting the visibility of calcifications, thereby aligning with the overarching objective of assisting the detection of calcifications within the scope of this study.

#### 4. CONCLUSION

This study has successfully proposed the AFWMF that can exceed the overall performance of the conventional method which known as FWMF. The AFWMF allows for easy manipulation of parameter settings to achieve the desired enhancement characteristics on images, particularly in the detection of diseases in medical images, especially calcifications. The calcifications can easily be seen by using the FWMF which the parameter of range C as the threshold range in the fuzzy membership function with the PSNR and MAE value of 96.2268 and 0.0000636 respectively. However, the number of calcifications that shown in the images are manipulated by the filter that its size is different from the original images. Hence, the future works need to be done to ensure that the calcifications size are not affected by the filter that might affect the classifications of calcifications either microcalcifications of macrocalcifications.

#### ACKNOWLEDGEMENTS

The authors acknowledge the financial support provided by the Ministry of Higher Education Grant Scheme (FRGS) for research project titled "A new cascaded convolutional neural network model for deblurring and contrast enhancement of extremely dense breast tissue in digital breast tomosynthesis images" with reference number FRGS/1/2021/TK0/UITM/02/19. Ethics approval for the study was obtained from Universiti Sains Malaysia (USM/JEPeM/21090622), ensuring the research adheres to ethical guidelines. The authors would like to extend their gratitude to the members of the Advanced Rehabilitation Engineering in Diagnostic and Monitoring Research Group (AREDiM), and the Centre for Electrical Engineering Studies at Universiti Teknologi MARA, Cawangan Pulau Pinang. Additionally, the authors would like to express their appreciation to the Integrative Pharmacogenomics Institute (iPROMISE) at UiTM Puncak Alam for their valuable assistance and guidance during the fieldwork. Lastly, the authors express their appreciation to Univeristi Teknologi MARA, Cawangan Pulau Pinang, for their significant administrative and financial support, which contributed to the successful executions of this research work.




#### REFERENCES

- [1] "Breast cancer: causes, stage, diagnosis & treatment," Cleveland Clinic. Accessed: Dec. 26, 2021. [Online]. Available: <https://my.clevelandclinic.org/health/diseases/3986-breast-cancer>
- [2] "Breast calcifications: causes, types, treatment & tests," Accessed: Dec. 26, 2021. [Online]. Available: <https://my.clevelandclinic.org/health/diseases/17802-breast-calcifications>
- [3] T. M. A. Basile *et al.*, "Microcalcification detection in full-field digital mammograms: a fully automated computer-aided system," *Physica Medica*, vol. 64, pp. 1–9, Aug. 2019, doi: 10.1016/j.ejmp.2019.05.022.
- [4] A. Rodriguez-Ruiz *et al.*, "New reconstruction algorithm for digital breast tomosynthesis: better image quality for humans and computers," *Acta Radiologica*, vol. 59, no. 9, pp. 1051–1059, Sep. 2018, doi: 10.1177/0284185117748487.
- [5] Y. Park *et al.*, "Evaluation of the image quality in digital breast tomosynthesis (DBT) employed with a compressed-sensing (CS)-based reconstruction algorithm by using the mammographic accreditation phantom," *Nuclear Instruments and Methods in Physics Research Section A: Accelerators, Spectrometers, Detectors and Associated Equipment*, vol. 804, pp. 72–78, Dec. 2015, doi: 10.1016/j.nima.2015.09.042.
- [6] J. S. Choi, B.-K. Han, E. Y. Ko, G. R. Kim, E. S. Ko, and K. W. Park, "Comparison of synthetic and digital mammography with digital breast tomosynthesis or alone for the detection and classification of microcalcifications," *European Radiology*, vol. 29, no. 1, pp. 319–329, Jan. 2019, doi: 10.1007/s00330-018-5585-x.
- [7] P. S. Sujlana, M. Mahesh, S. Vedantham, S. C. Harvey, L. A. Mullen, and R. W. Woods, "Digital breast tomosynthesis: image acquisition principles and artifacts," *Clinical Imaging*, vol. 55, pp. 188–195, May 2019, doi: 10.1016/j.clinimag.2018.07.013.
- [8] N. Tirada *et al.*, "Digital breast tomosynthesis: physics, artifacts, and quality control considerations," *RadioGraphics*, vol. 39, no. 2, pp. 413–426, Mar. 2019, doi: 10.1148/rg.2019180046.
- [9] R. K. Samala *et al.*, "Detection of microcalcifications in breast tomosynthesis reconstructed with multiscale bilateral filtering regularization," C. L. Novak and S. Aylward, Eds., Mar. 2013, p. 86701L. doi: 10.1117/12.2008230.




- [10] X. Lai, W. Yang, and R. Li, "DBT masses automatic segmentation using U-Net neural networks," *Computational and Mathematical Methods in Medicine*, vol. 2020, pp. 1–10, Jan. 2020, doi: 10.1155/2020/7156165.
- [11] R. K. Samala, H.-P. Chan, Y. Lu, L. M. Hadjiiski, J. Wei, and M. A. Helvie, "Computer-aided detection system for clustered microcalcifications in digital breast tomosynthesis using joint information from volumetric and planar projection images," *Physics in Medicine and Biology*, vol. 60, no. 21, pp. 8457–8479, Nov. 2015, doi: 10.1088/0031-9155/60/21/8457.
- [12] R. K. Samala, H.-P. Chan, Y. Lu, L. M. Hadjiiski, J. Wei, and M. Helvie, "Digital breast tomosynthesis: effects of projection-view distribution on computer-aided detection of microcalcification clusters," S. Aylward and L. M. Hadjiiski, Eds., Mar. 2014, p. 90350Y. doi: 10.1117/12.2043513.
- [13] M. U. Ghani *et al.*, "Development and preclinical evaluation of a patient-specific high energy x-ray phase sensitive breast tomosynthesis system," *Medical Physics*, vol. 48, no. 5, pp. 2511–2520, May 2021, doi: 10.1002/mp.14743.
- [14] R. K. Samala, H.-P. Chan, L. M. Hadjiiski, K. Cha, and M. A. Helvie, "Deep-learning convolution neural network for computer-aided detection of microcalcifications in digital breast tomosynthesis," G. D. Tourassi and S. G. Armato, Eds., Mar. 2016, p. 97850Y. doi: 10.1117/12.2217092.
- [15] N. Xu, S. Yi, P. Mendonca, T. Tian, R. Samala, and H.-P. Chan, "False positive reduction of microcalcification cluster detection in digital breast tomosynthesis," S. Ourselin and M. A. Styner, Eds., Mar. 2014, p. 90342N. doi: 10.1117/12.2043763.
- [16] R. K. Samala, H.-P. Chan, Y. Lu, L. M. Hadjiiski, J. Wei, and M. A. Helvie, "Digital breast tomosynthesis: computer-aided detection of clustered microcalcifications on planar projection images," *Physics in Medicine and Biology*, vol. 59, no. 23, pp. 7457–7477, Dec. 2014, doi: 10.1088/0031-9155/59/23/7457.
- [17] S. N. Sulaiman, M. H. Normazli, N. A. Harron, N. K. A. Karim, K. A. Ahmad, and Z. H. C. Soh, "A convolutional neural network model for image enhancement of extremely dense breast tissue in digital breast tomosynthesis images," in *2022 IEEE 12th International Conference on Control System, Computing and Engineering (ICCSCE)*, IEEE, Oct. 2022, pp. 153–157. doi: 10.1109/ICCSCE54767.2022.9935647.
- [18] G. Zhang, J. Lin, E. Cao, Y. Pang, and W. Sun, "A medical endoscope image enhancement method based on improved weighted guided filtering," *Mathematics*, vol. 10, no. 9, p. 1423, Apr. 2022, doi: 10.3390/math10091423.
- [19] P. K. Mall and P. K. Singh, "BoostNet: a method to enhance the performance of deep learning model on musculoskeletal radiographs X-ray images," *International Journal of System Assurance Engineering and Management*, vol. 13, no. S1, pp. 658–672, Mar. 2022, doi: 10.1007/s13198-021-01580-3.
- [20] K. Panetta, Yicong Zhou, S. Agaian, and Hongwei Jia, "Nonlinear unsharp masking for mammogram enhancement," *IEEE Transactions on Information Technology in Biomedicine*, vol. 15, no. 6, pp. 918–928, Nov. 2011, doi: 10.1109/TITB.2011.2164259.
- [21] S. A. Saifudin, S. N. Sulaiman, N. K. A. Karim, M. K. Osman, I. S. Isa, and N. A. Harron, "A comparative study of unsharp masking filters for enhancement of digital breast tomosynthesis images," in *2022 IEEE 12th International Conference on Control System, Computing and Engineering (ICCSCE)*, IEEE, Oct. 2022, pp. 147–152. doi: 10.1109/ICCSCE54767.2022.9935638.
- [22] D. Ngo, S. Lee, and B. Kang, "Nonlinear unsharp masking algorithm," in *2020 International Conference on Electronics, Information, and Communication (ICEIC)*, IEEE, Jan. 2020, pp. 1–6. doi: 10.1109/ICEIC49074.2020.9051376.
- [23] S. A. Saifudin, S. N. Sulaiman, M. K. Osman, I. S. Isa, and N. K. Noor, "Fuzzy weighted median filter with unsharp masking for enhancement of Dbt images in breast cancer detection," *Journal of Health and Translational Medicine*, vol. 2023, no. Special Issue 1, pp. 172–181, 2023, doi: 10.22452/jumec.sp2023no1.17.
- [24] S. Sulaiman and N. Mat Isa, "Denoising-based clustering algorithms for segmentation of low level salt-and-pepper noise-corrupted images," *IEEE Transactions on Consumer Electronics*, vol. 56, no. 4, pp. 2702–2710, Nov. 2010, doi: 10.1109/TCE.2010.5681159.
- [25] K. Toh, H. Ibrahim, and M. Mahyuddin, "Salt-and-pepper noise detection and reduction using fuzzy switching median filter," *IEEE Transactions on Consumer Electronics*, vol. 54, no. 4, pp. 1956–1961, Nov. 2008, doi: 10.1109/TCE.2008.4711258.

## BIOGRAPHIES OF AUTHORS






**Syafiqah Aqilah Saifudin**    obtained her B.Eng. Hons in Electrical and Electronics Engineering from Universiti Teknologi MARA in 2017 and M.Sc. in Science from the same university in 2021. She is now doing her Ph.D. in Electrical Engineering, focusing on medical imaging at the university. Her research interests include image processing and image filtering in medical images. She can be contacted at email: syafiqahsaifudin98@gmail.com.






**Siti Noraini Sulaiman**    (Senior Member, IEEE) received the B.Eng. degree (Hons.) in Electrical and Electronics and the M.Sc. degree in Electrical and Electronics Engineering (medical imaging) from Universiti Sains Malaysia, in 2000 and 2003, respectively, and the Ph.D. degree in imaging from the School of Electrical and Electronics Engineering, Universiti Sains Malaysia, in 2012. She joined the Faculty of Electrical Engineering, Universiti Teknologi MARA (UiTM), Penang Branch, Penang, Malaysia, as a contract lecturer, in 2002. She is currently an Associate Professor heading the Advanced Rehabilitation Engineering in Diagnostic and Monitoring Research Group (AREDiM), School of Electrical Engineering, College of Engineering, UiTM. She has published numerous research articles in international journals and conference proceedings. Her research interests include intelligent systems, image processing, neural networks for medical applications, and algorithms. She can be contacted at email: sitinoraini@uitm.edu.my.






**Muhammad Khusairi Osman**    graduated from Universiti Sains Malaysia with a B.Eng. Degree in Electrical and Electronic Engineering in 2000 and M.Sc. in Electrical and Electronic Engineering in 2004. In 2014, he received his Ph.D. in Medical Electronic Engineering from Universiti Malaysia Perlis (UniMAP), Malaysia. He is currently a senior lecturer at the Faculty of Electrical Engineering, Universiti Teknologi MARA (UiTM), Malaysia. Image processing, pattern recognition, and artificial intelligence are among his research interests. He can be contacted at email: [khusairi@uitm.edu.my](mailto:khusairi@uitm.edu.my).






**Iza Sazanita Isa**    received her bachelor's in Electrical Engineering from the Universiti Teknologi MARA, Malaysia in 2004 and the M.Sc. degree from the Universiti Sains Malaysia, Malaysia in 2008. Since 2009, she joined Universiti Teknologi MARA, Penang Campus, Malaysia as young lecturer and has been promoted as senior lecturer with the School of Electrical Engineering, College of Engineering, Universiti Teknologi MARA (UiTM), Penang branch, in 2013. She pursues her Ph.D. in Electrical Engineering under the SLAB/SLAI scholarship and graduated in 2018. Currently she is joining Universiti Sains Malaysia (USM), Malaysia as postdoctoral fellowship under School of Computer Sciences. She is attached to department of Control System Engineering at the faculty. She is also the members of AREDiM research group, the head of research group RIDyLT and actively involved in teaching and learning research. Her research interest includes the model development using image processing and artificial intelligence. She can be contacted at email: [izasazanita@uitm.edu.my](mailto:izasazanita@uitm.edu.my).



**Noor Khairiah A Karim**    received her bachelor degree in Medicine, bachelor degree in Surgery (MBBS), and Master of Radiology (MRad) from the University of Malaya, Malaysia. She then obtained her Fellowship in Cardiac Imaging from the National Heart Center Singapore. She is currently a Senior Medical Lecturer of the Regenerative Medicine Cluster, and a Consultant Radiologist at the Advanced Medical and Dental Institute, Universiti Sains Malaysia. Her current research areas include medical image processing and analysis with a special interest in cardiac, breast and brain imaging. She can be contacted at email: [drkhairiah@usm.my](mailto:drkhairiah@usm.my).



**Nur Athiqah Harron**    is a senior lecturer at the Universiti Teknologi MARA Cawangan Pulau Pinang. Nur Athiqah obtained her Bachelor of Electrical Engineering (Computer) from Universiti Teknologi Malaysia in 2007 and MSc in Electronic System Design Engineering from Universiti Sains Malaysia in 2011. She currently is doing her Ph.D. at Universiti Teknologi MARA Cawangan Pulau Pinang. Her research focuses on the image processing of the medical image, specifically in analysing DBT image enhancement using deep learning. She can be contacted at email: [nurathiqah742@uitm.edu.my](mailto:nurathiqah742@uitm.edu.my).